



Photonic Floquet Topological Insulators in Atomic Ensembles

Yiqi Zhang¹, Milivoj R. Belić², Min Xiao^{3,4}, and Yanpeng Zhang¹

¹XJTU, Xi'an 710049, China, ²TAMUQ, 23874 Doha, Qatar, ³UARK, Arkansas 72701, USA, ⁴NJU, Nanjing 210093, China

Abstract

- A photonic Floquet topological insulator (PFTI) in an atomic ensemble is demonstrated numerically and theoretically.
- The interference of three coupling fields will split energy levels periodically, to form a periodic refractive index structure with honeycomb profile that can be adjusted by different frequency detunings and intensities of the coupling fields.
- When the honeycomb lattice sites are helically ordered along the propagation direction, gaps open at Dirac points, and one obtains a PFTI in an atomic vapor.
- The appearance of Dirac cones and the formation of a photonic Floquet topological insulator can be shut down by the third-order nonlinear susceptibility and opened up by the fifth-order one.

Introduction

Recently, topological insulators (TIs) have attracted much attention, since a TI, as a new phase of matter, only allows conducting electrons to exist on the surfaces, and the moving electrons are not affected by defects or disorder. There are edge states in TIs that lie in a bulk energy gap in momentum space and are spatially localized on the boundaries of the TIs. The edge states are predicted to be useful in performing quantum computations. Topological insulators, as well as some graphene-based structures, have also found potential applications in optical modulators and optical diodes. Photonic topological insulators (PTIs), fabricated by using metamaterials or helical waveguides [1], can break the time-reversal symmetry and lead to oneway edge states, which are robust against defects.

So far, research on PTIs has been mostly based on graphene-like structures. A honeycomb lattice also exhibits certain graphene-like properties and can be obtained by using the femtosecond laser writing technique or the three-beam interference method [2-5]. The first method is valid only in solid materials, whereas the second method can be used in both solid and gaseous materials. We note that the three-beam interference will generally induce a hexagonal lattice instead of the honeycomb lattice. However, the corresponding refractive index modulation will exhibit a honeycomb profile in a saturable nonlinear medium or an atomic vapor. The interference pattern (in the form of a hexagonal lattice) produced by the three-beam interference will exhibit many pairs of singularities, and the band structure of the corresponding refractive index change (in the form of a honeycomb lattice) will feature conical singularities at the corners of the first Brillouin zone. In an atomic (e.g. rubidium) vapor, when the three-beam interference pattern serves as the dressing field, the dressed atomic system will exhibit controllable optical properties, which were extensively investigated in the past decade.

The model

- An inverted Y-type electromagnetically induced transparency (EIT) system, as shown in Fig. 1(a).
- E_p probes the transition $|0\rangle \rightarrow |1\rangle$, E_2 drives the transition $|1\rangle \rightarrow |2\rangle$, and E_3 connects $|1\rangle \rightarrow |3\rangle$.
- If three coupling fields are used with the same frequency and launched along the same direction z , the resulting Rabi frequency of such optically induced interference pattern can be written as

$$G = \sum_{i=1}^3 G_2 \exp[ik_2(x\cos\theta_i + y\sin\theta_i)],$$

- $\theta_i = [0, 2\pi/3, 4\pi/3]$ are the relative phases of the three laser beams,
- k_2 is the wavenumber of the coupling fields,
- $G_2 = \mu_{12}E_2/\hbar$ represents the Rabi frequencies of the coupling fields where μ_{12} is the electric dipole moment.
- Level $|1\rangle$ can be dressed by the coupling fields and split into two sublevels $|+\rangle$ and $|-\rangle$, as shown in Fig. 1(b).

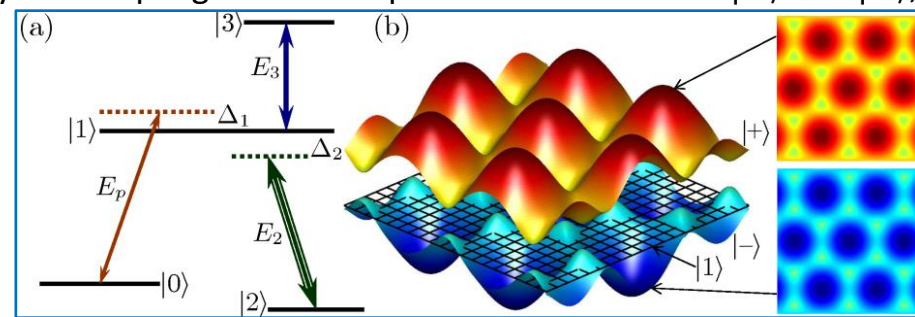


Figure 1. Schematic diagram.

- The susceptibility can be written as

$$\chi(x, y) = \chi_p^{(1)} + \chi_p^{(3)}|E_2|^2 + \chi_p^{(5)}|E_2|^4,$$

- The linear, third-order, and fifth-order susceptibilities are

$$\chi_p^{(1)} = \frac{iN\mu_{10}^2}{\hbar\epsilon_0(d_{10} + d_{20})}, \chi_p^{(3)}|E_2|^2 = -\frac{iN\mu_{10}^2G_2^2}{\hbar\epsilon_0[d_{20}(d_{10} + \frac{|G_2|^2}{d_{20}})]}, \chi_p^{(5)}|E_2|^4 = \frac{iN\mu_{10}^2G_2^4}{\hbar\epsilon_0[d_{20}^2(d_{10} + \frac{|G_2|^2}{d_{20}})^2]}$$

- N is the atomic density, μ_{10} the electric dipole moment, $d_{10} = \Gamma_{10} + i\Delta_1$ and $d_{20} = \Gamma_{20} + i(\Delta_1 - \Delta_2)$ the complex relaxation rates.
- Γ_{ij} is the decay rate between $|i\rangle$ and $|j\rangle$, $\Delta_1 = \Omega_{10} - \omega_p$ and $\Delta_2 = \Omega_{12} - \omega_2$ are the frequency detunings.
- Ω_{ij} is the transition frequency between $|i\rangle$ and $|j\rangle$, and ω_p (ω_2) is the frequency of the probe (coupling) field.

Refractive index change & Photonic band structure

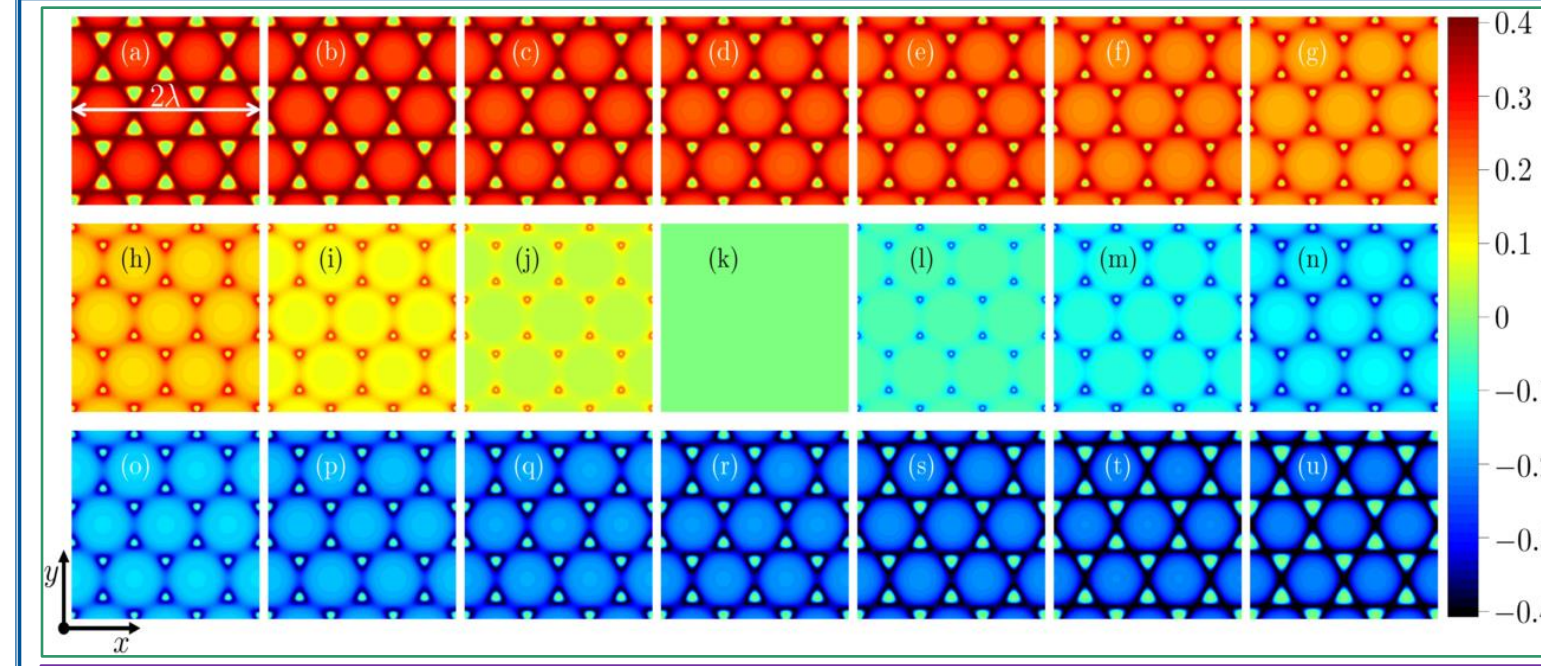


Figure 2. Refractive index (RI) $\Delta n(x, y)$ with $\Delta_1 = -\Delta_2 = -10$ MHz (a), -9 MHz (b), -8 MHz (c), -7 MHz (d), -6 MHz (e), -5 MHz (f), -4 MHz (g), -3 MHz (h), -2 MHz (i), -1 MHz (j), 0 (k), 1 MHz (l), 2 MHz (m), 3 MHz (n), 4 MHz (o), 5 MHz (p), 6 MHz (q), 7 MHz (r), 8 MHz (s), 9 MHz (t), and 10 MHz (u).

- $\Delta_1 = -\Delta_2 < 0$: Honeycomb lattice is composed of circle-like structures, because the RI at the sites is the smallest and the RI immediately around the sites is the biggest.
- $\Delta_1 = -\Delta_2 = 0$: No honeycomb lattice - homogeneous medium.
- $\Delta_1 = -\Delta_2 > 0$: Honeycomb lattice is composed of the sites, because the RI at the site is the biggest.

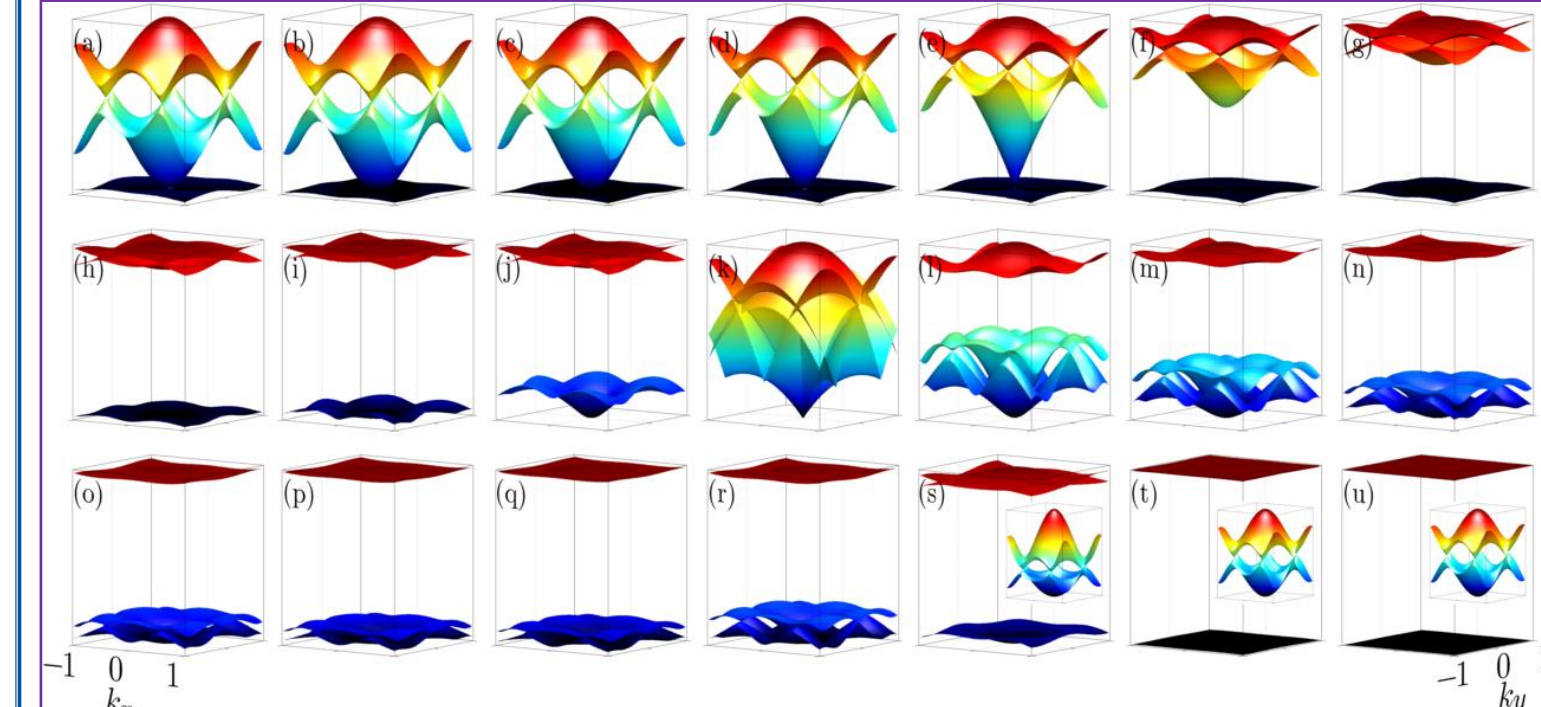


Figure 3. Photonic band structures corresponding to Fig. 2. Insets in (s)-(u) only show the upper two bands.

- $\Delta_1 = -\Delta_2 < 0$: There are always Dirac cones between upper two bands.
- $\Delta_1 = -\Delta_2 = 0$: No Dirac cone.
- $\Delta_1 = -\Delta_2 > 0$: Appearance of Dirac cones between upper two bands can be controlled by adjusting frequency detunings.

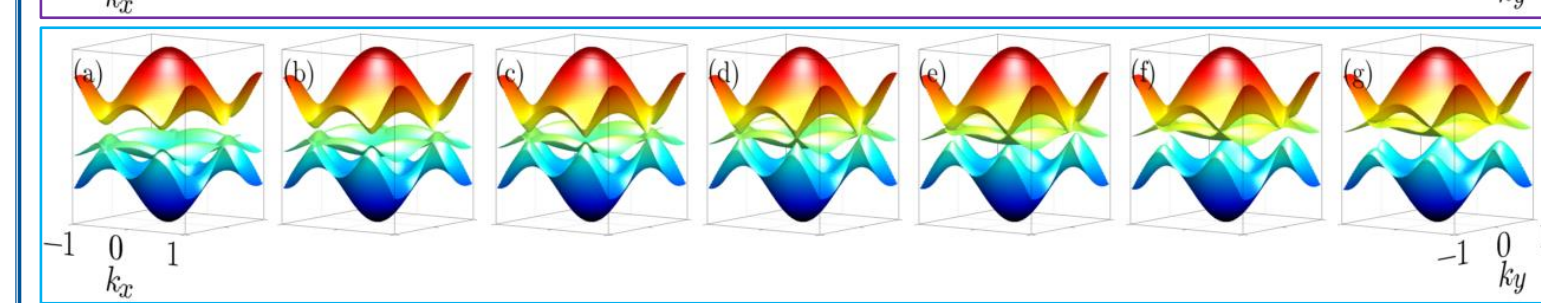


Figure 4. Photonic band structures corresponding to $\Delta_1 = -\Delta_2 = 7.63$ MHz (a), 7.64 MHz (b), 7.65 MHz (c), 7.66 MHz (d), 7.67 MHz (e), 7.68 MHz (f), and 7.69 MHz (g), respectively.

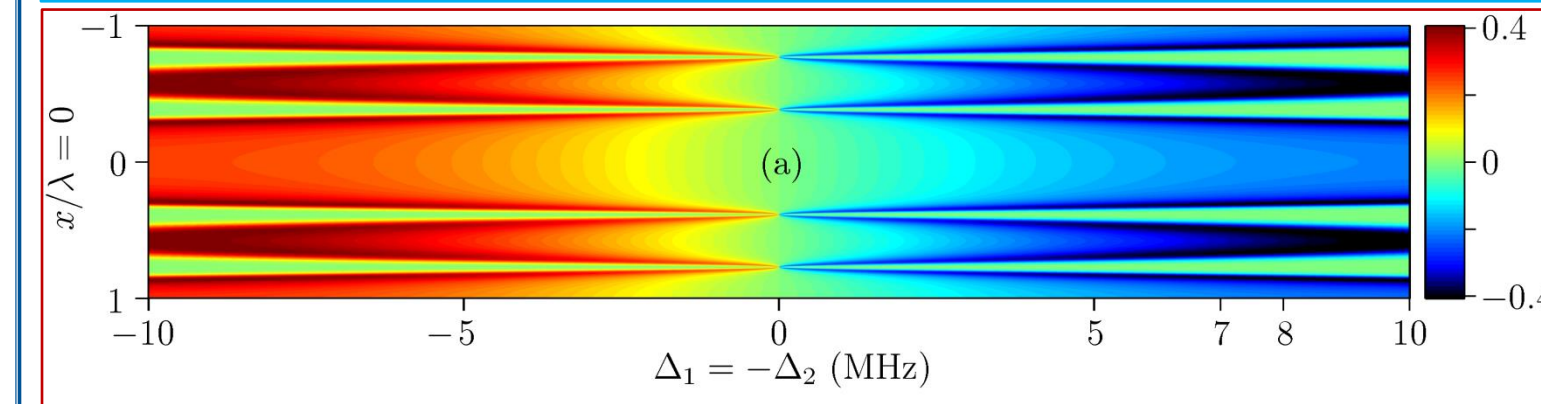
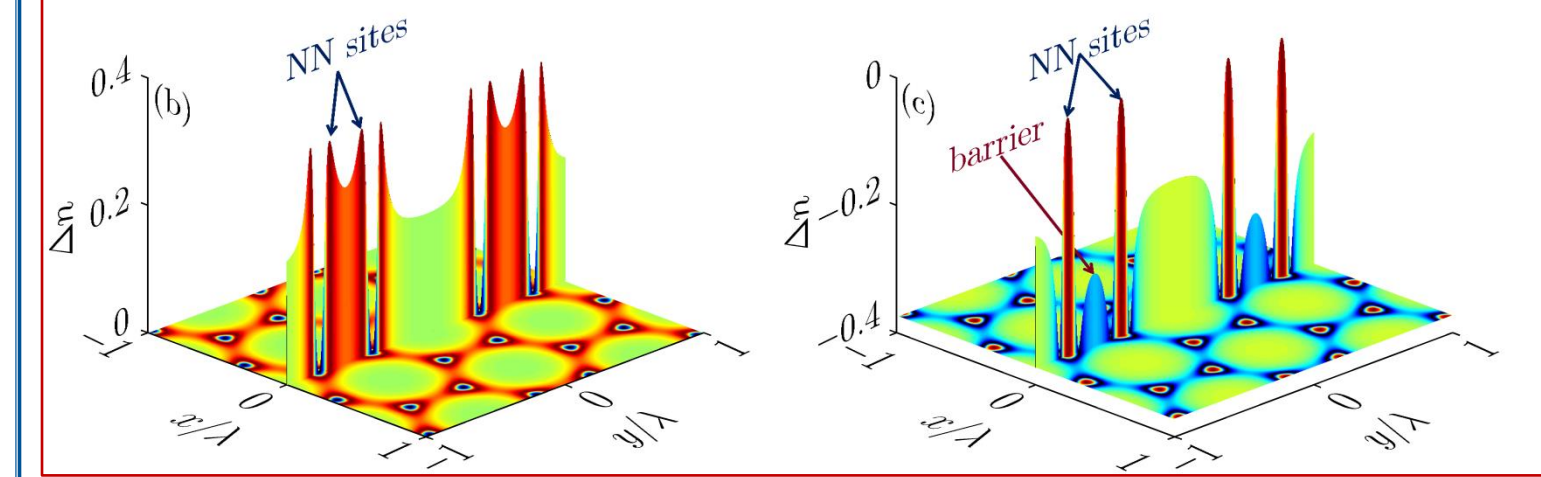


Figure 5. (a) The RI change along the cross section $x = 0$ versus different frequency detunings. (b) RI change in the $x = 0$ plane, corresponding to Fig. 2(f). (c) Same as (b), but corresponding to Fig. 2(p).



- $\Delta_1 = -\Delta_2 < 0$: No potential barrier between lattice sites.
- $\Delta_1 = -\Delta_2 > 0$: Potential barrier blocks the hopping between nearest neighbors sites. With the increasing of the frequency detuning, the barrier decreases, and the blockade effect also weakens.

Photonic Floquet topological insulator

- Mathematical realization: Transform the coordinates with $x' = x + R\cos(\omega z)$, $y' = y + R\sin(\omega z)$ and $z' = z$ with R the radius of the helix and ω the frequency of rotation.
- Potential experimental method - nonlinear phase shift (NPS) modulation: E_3 in Fig. 1 splits $|+\rangle$ into $|+\pm\rangle$. In cylindrical coordinate, the NPS can be written as $S_{NL}(r, \phi, z) = 2k_2 n_2^x I_3 z \exp[r^2 + I^2 + 2rI\cos(\phi - \phi')]/n_0$, in which n_2^x is the cross-Kerr nonlinear index from E_3 .

- The NPS will induce a transverse vector $\delta \mathbf{k}_\perp(r, \phi) = \hat{r} \frac{\partial S_{NL}}{\partial r} + \hat{\phi} \frac{1}{r} \frac{\partial S_{NL}}{\partial \phi} = \mathbf{k}_r + \mathbf{k}_\phi$, with \hat{r} and $\hat{\phi}$ being the unit vectors.
- \mathbf{k}_r and \mathbf{k}_ϕ will drive the honeycomb lattice move radially and azimuthally along with z .

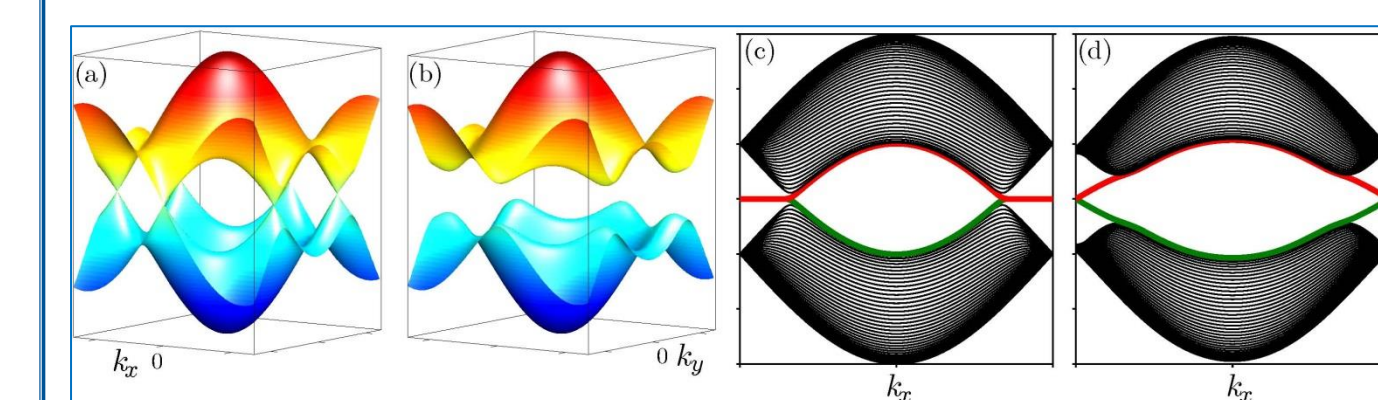


Figure 6. Band structures when the honeycomb waveguides are not spiraling (a) and spiraling (b). (c) Edge band structure of the strained honeycomb waveguides with zigzag boundaries. (d) Same as (c), but corresponding to (b).

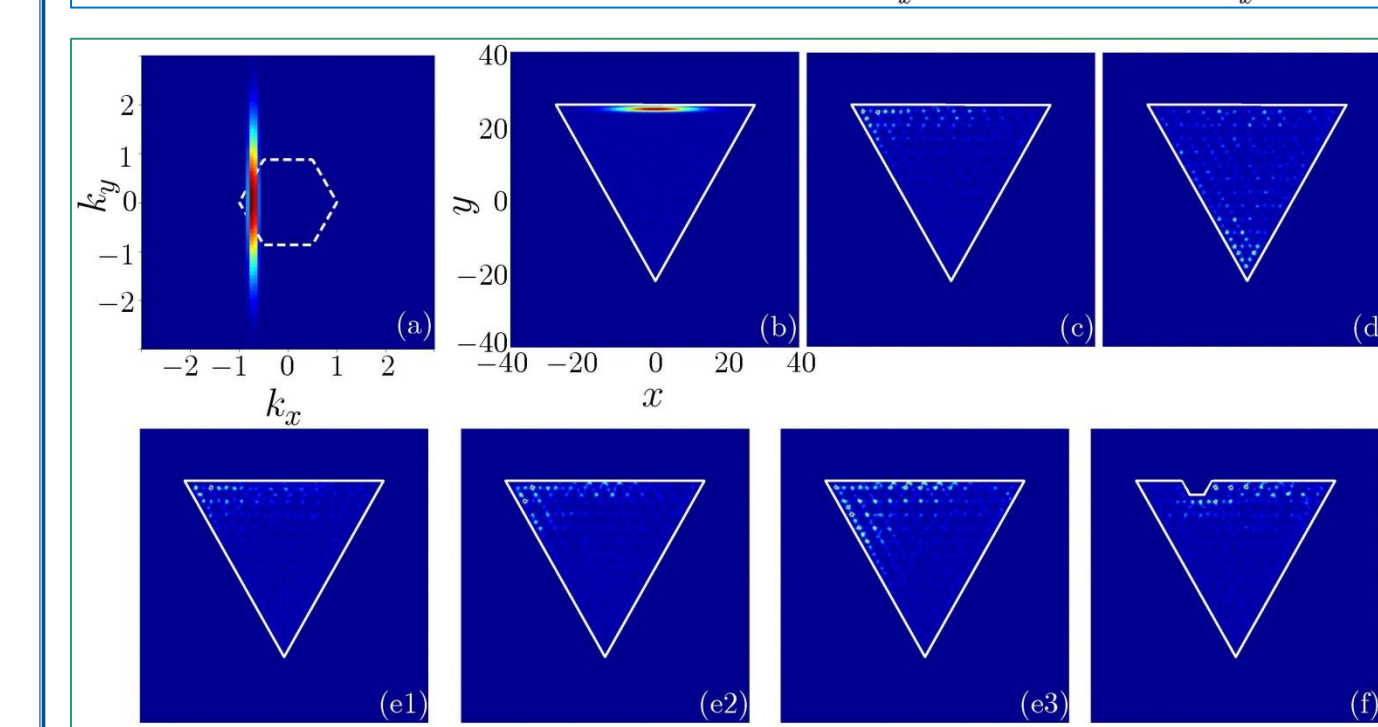


Figure 7. (a) Input beam in Fourier space. (b-d) Simulated probe beam intensities at $z = 0$, $z \approx 6.3 \mu\text{m}$, and $z \approx 18.6 \mu\text{m}$, respectively. The inverted triangle presents the PFTI with modulated RI and zigzag boundaries. The parameters are $\Delta_1 = -\Delta_2 = -1$ MHz, $V_0 = 150$, $R \approx 24.8$ nm, and $\frac{\omega}{2\pi} \approx 0.8$ GHz (the period is ~ 1.2 nm). (e1-e3) Same as (c) but under $\Delta_1 = -\Delta_2 = -11$ MHz, -9 MHz, and -8 MHz, respectively. (f) Beam propagates to $z \approx 4.7 \mu\text{m}$ with a disorder.

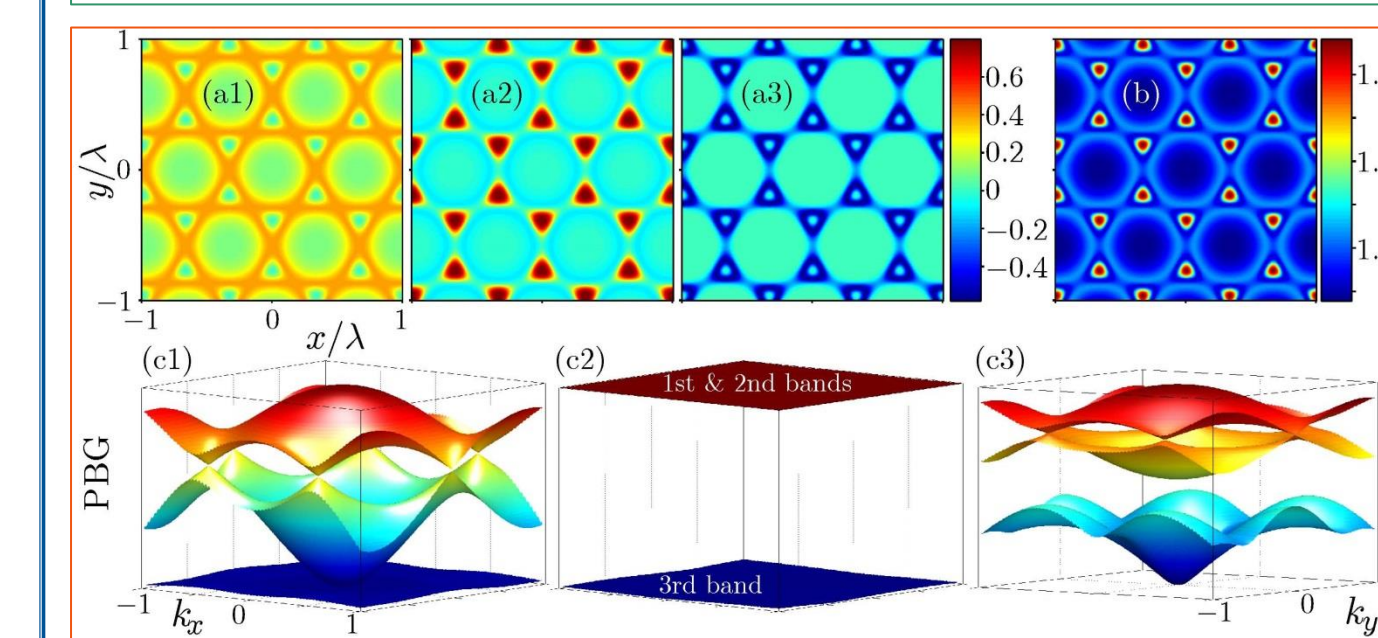


Figure 8. (a1-a3) Real parts of $\chi_p^{(1)}$, $\chi_p^{(3)}|E_2|^2$ and $\chi_p^{(5)}|E_2|^4$, respectively. (b) RI with $\chi_p^{(1)}$, $\chi_p^{(3)}|E_2|^2$ and $\chi_p^{(5)}|E_2|^4$ considered. Parameters are $\Delta_1 = 0$, $\Delta_2 = 10$ MHz and $G_2 = 10$ MHz. (c) PBG structures for RI with $\chi_p^{(1)}$ (c1), $\chi_p^{(1)} + \chi_p^{(3)}|E_2|^2$ (c2), and $\chi_p^{(1)} + \chi_p^{(3)}|E_2|^2 + \chi_p^{(5)}|E_2|^4$ (c3) considered, respectively.

Conclusions

- We have proposed a scheme for construction of PFTIs in multi-level atomic vapor ensembles.
- The formed PFTIs in atomic ensembles can be easily controlled and reconfigured by adjusting the frequency detunings, coupling field intensities, and high-order nonlinear susceptibilities.
- The PFTIs should also exist in other types of multi-level atomic systems.

Acknowledgement and References

National Basic Research Program of China (2012CB921804); National Natural Science Foundation of China (61308015, 11474228); China Postdoctoral Science Foundation (2014T70923, 2012M521773); Key Scientific and Technological Innovation Team of Shaanxi Province (2014KCT-10); National Science Foundation of Shaanxi Province (2014JQ8341); Qatar National Research Fund (a member of the Qatar Foundation) (NPRP 6-021-1-005).

References:

- [1] M.C. Rechtsman, J.M. Zeuner, Y. Plotnik, et al. Nature 496, 196-200 (2013).
- [2] Y. Plotnik, M.C. Rechtsman, D. Song, et al. Nat. Mater. 13, 57-62 (2014).
- [3] D. Song, V. Paltoglou, S. Liu, et al. Nat. Commun. 6, 6272 (2015).
- [4] Y. Q. Zhang, Z. K. Wu, M. R. Belić, et al. Laser Photonics Rev. 9, 331-338 (2015).
- [5] Y. Q. Zhang, X. Liu, M. R. Belić, et al. Ann. Phys. (under review).